THE ASTROPHYSICAL JOURNAL, 454:316–326, 1995 November 20

THE H II REGION SHARPLESS 170: A MULTISCALE ANALYSIS OF THE Hα VELOCITY FIELD

MARC-ANTOINE MIVILLE-DESCHÊNES AND GILLES JONCAS
Département de Physique, Observatoire Astronomique du Mont Mégantic, Université Laval Sainte-Foy, Québec G1K 7P4, Canada
AND
DANIEL DURAND
Dominion Astrophysical Observatory, National Research Council of Canada, 5071 W. Saanich Road, Victoria, BC V8X 4M6, Canada
Received 1994 October 18; accepted 1995 May 11

ABSTRACT

A total of 12,695 Hα radial velocities were measured across the H II region Sh 170 using a Fabry-Perot camera. The mean V_{LSR} of the ionized gas is -50.10 ± 0.08 km s^{-1} with a velocity dispersion of 8.70 ± 0.05 km s^{-1}. Sh 170 has a blueshift of 6.4 km s^{-1} with respect to the associated molecular cloud. The nebula is density bounded on all visible sides, indicating that the H II region is seen in front of the molecular cloud. The velocity field can be explained as an expansion of the ionized gas away from the molecular cloud toward the observer. A north-south velocity gradient of 1.4 km s^{-1} pc is also observed. The locus of the less negative velocity ($V_{LSR} \approx -45$ km s^{-1}) coincides with the molecular cloud's position. Several kinematical and morphological aspects of Sh 170 are in good agreement with the "Champagne" phase model. Sh 170 has a ~ 2 pc cavity devoid of ionized gas approximately centered on the ionizing star which can be explained by the action of a stellar wind. The large number of velocity measurements allowed a systematic analysis of velocity fluctuations in Sh 170. The relation between centroid velocity dispersion σ_c and scale l was derived. The two-point autocorrelation (C) and structure (S) functions were used; these are reliable tools for the investigation of the statistical properties of fluctuating gas motions. It was found that velocity correlation occurs at scales smaller than 0.7 pc in Sh 170. The e-folding length of the autocorrelation function (the correlation length) is 0.03 ± 0.02 pc, and a power-law relation between S and scale was obtained: $S(\tau) \propto \tau^{0.8 \pm 0.1}$. An interpretation of these results in terms of turbulence is presented.

Subject headings: H II regions — ISM: individual (Sharpless 170) — ISM: kinematics and dynamics — turbulence

1. INTRODUCTION

H II regions have their origin in the complex and ill-defined massive star formation process that occurs in molecular clouds. Diffuse nebulae are of course observed near such clouds and dynamical models such as the "Blister" model (Israel 1978) or "Champagne" model (Tenorio-Tagle 1979) predicted an expansion phase of the ionized gas from the parent cloud. Detailed velocity maps of H II regions (Wilson et al. 1959; Fishel & Feibelman 1973; Mufson et al. 1981; Fountain, Gary, & O'Dell 1983a, b; Joncas & Roy 1984b, 1986; Joncas, Durand, & Roger 1992) revealed large-scale velocity trends interpreted in term of gas flows leaving molecular regions, as suggested by the models.

On the other hand, actual modelization does not adequately meet the small-scale analysis made on H II region velocity fields (Yorke, Tenorio-Tagle, & Bodenheimer 1984; Joncas et al. 1992). In addition, characteristics of the interstellar medium (Kaplan & Pikelner 1970, p. 336) clearly indicate that it must be described in terms of turbulent flows (Scalo 1987). Observationally, it has been suggested that the relation between average velocity dispersion and scale found in molecular clouds (Myers 1987, and references therein) and H II regions (Joncas & Roy 1984b, 1986) could be attributed to turbulence. Analysis of velocity fields with two-point statistical functions like the autocorrelation function and the structure function confirmed the presence of turbulence in molecular clouds (Kleiner & Dickman 1985; Miesch & Bally 1994) and H II regions (Roy & Joncas 1985; Joncas & Boily 1995; O'Dell 1986; O'Dell & Castañeda 1987). These statistical functions are better suited to investigate multiscale properties of a flow and are more reliable for the study of turbulence than the dispersion-scale relation (Scalo 1984).

The velocity field analysis of the H II region Sh 170 follows other similar studies of H II regions like Sh 158 and M42 (Boily 1993). The aim of this global project is to interpret numerous radial velocity measurements to help refine kinematical models of H II regions and to describe their turbulent behavior. Sh 170 was chosen for its apparent morphological simplicity; we present background information on this nebula in § 2. The observations are described in § 3, and the Hα velocity field resulting from the data processing is presented in § 4. Section 5 discusses a kinematical model for Sh 170 considering the Champagne model and a strong stellar wind. Finally, small-scale behavior of the velocity field is discussed in terms of turbulence in § 6.

2. BACKGROUND INFORMATION ON Sh 170

Sh 170 [$\alpha(1950) = 23^h59^m00^s$, $\delta(1950) = 64°20'00''$] (Sharpless 1959) is a faint H II region with a diameter of $\sim 20'$. Sh 170 is located in the Perseus arm ($l = 117.57$, $b = 2.26$) and is associated with a molecular cloud detected by Fich & Blitz (1984) at a mean V_{LSR} of -43.7 km s^{-1}. This velocity implies a kinematical distance of 2.30 ± 0.70 kpc for this gas complex. Wouterloot & Brand (1989) derived kinematical heliocentric distances for *IRAS* sources using CO observations, obtaining 4.60 kpc for Sh 170. This discrepancy comes from the use of a different rotation curve for the Milky Way. Wide-band photometry made by Lahulla (1985) gives a distance of 2.3 kpc for the only exciting star of Sh 170: DM 63°2093. Hunter & Massey (1900) classified DM 63°2093 as an O8 V star of 31

$M_\odot$. Simulating BV filters, they determined a distance of 4.0 kpc for the star. In this paper we adopt the photometric distance of 2.3 kpc, since noncircular motions in the Perseus arm affects kinematical distance measurements.

Among other H II regions, Fich, Treffers, & Dahl (1990) made Hα observations of Sh 170 using a Fabry-Perot (F-P) spectrometer with an aperture of 2′. Their profile is centered at $V_{LSR} = -54.6 \pm 0.3$ km s^{-1} and has a line width $\Delta V = 29.3 \pm 0.5$ km s^{-1}. Figure 1 is a reproduction of the POSS red print containing Sh 170. The H II region has circular symmetry resembling a typical Strömgren sphere projected on the sky. Its outline is faint and ill defined, indicating that the nebula is density limited. Also visible on this print is the presence of an area near the exciting star where the nebular emission is fainter. Roger, Dewdney, & McCutcheon (1995) are preparing a paper on Sh 170 describing their radio (continuum and H I line) and millimeter (CO) observations. Their radio continuum map confirms the presence of an ionized gas trough in the H II region.

3. OBSERVATIONS AND DATA PROCESSING

The observations were made at the f/8 Ritchey-Chrétien focus of the Observatoire Astronomique du Mont Mégantic 1.60 m telescope in 1987, 1989, and 1993. It was equipped with an F-P camera built at Université Laval. It is composed of a focal reducer ($f/8 \rightarrow f3.4$) and a servo-stabilized F-P interferometer. A full description of the instrument is given in Joncas & Roy (1984a). The Hα line was observed using a narrow-band filter ($\delta\lambda = 11.8$ Å) centered at 6576 Å. The filter was tilted to the line center compensating for the air temperature and the blueshift of Sh 170. Two CCDs were used for this work: an RCA 320 × 512 in 1987 and 1989 and a Thompson 1024 × 1024 in 1993. These detectors had fields of view of 8′.8 × 5′.5 (pixel size = 1″.2) and 12′.8 × 12′.8 (pixel size = 0″.75), respectively. The F-P interferometer has a finesse of 30, an FWHM of 11 km s^{-1}, and a free spectral range of 392.4 km s^{-1} at Hα (6562.82 Å). It is optimized to operate between 4600 and 6800 Å.

The spatial coverage of Sh 170 (~20′) was done by dividing the object in four overlapping sections. Each section was partly scanned by taking Hα interferograms with three different spacings of the F-P interferometer. A total of 40 interferograms were taken on the sky (Table 1). A hydrogen calibration lamp was used to obtain rest frame interferograms. They were taken before and after each interferogram of Sh 170 to verify the stability of the F-P interferometer. Data analysis revealed that the F-P plate parallelism was always constant; a ring's radius was measured with a 0.05% precision.

The data processing was done using the Université Laval F-P package. The central idea of this package, written by

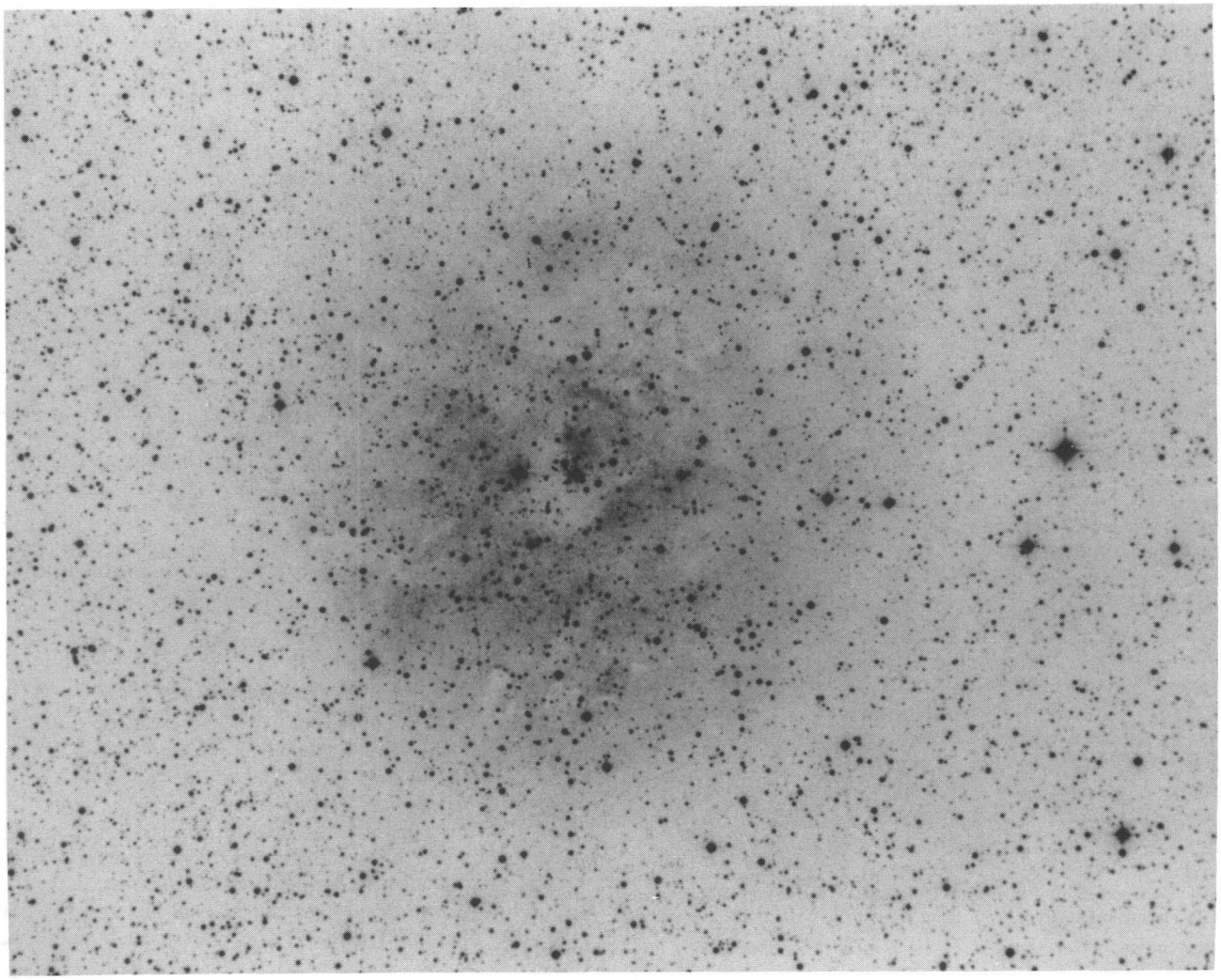

FIG. 1.—Reproduction of the Palomar Observatory Sky Survey (POSS) red print showing Sh 170 and its surroundings. Sh 170 covers 20′ on the sky.

TABLE 1

Hα INTERFEROGRAMS

Section	F-P Spacing	Exposure time (s)	Number of Images	Spatial Resolution (pc)
1.....	$z = 500$	2000	3	0.013
	$z = 620$	2000	3	0.013
	$z = 600$	3000	2	0.008
	$z = 600$	2000	1	0.008
2.....	$z = 500$	2000	4	0.013
	$z = 620$	2000	4	0.013
	$z = 740$	2000	4	0.013
3.....	$z = 500$	2000	4	0.013
	$z = 620$	2600	3	0.013
	$z = 740$	2600	3	0.013
4.....	$z = 500$	2600	3	0.013
	$z = 620$	2600	3	0.013
	$z = 740$	2600	3	0.013

Joncas & Durand, is to obtain the radial velocities by comparing the object's interferograms with those obtained with a source at rest (hydrogen calibration lamp). The velocities are computed using the relation

$$v = \frac{c}{2f^2}(R_2^2 - R_1^2),$$

where c is the speed of light, f is the focal length of the camera lens, R_2 is the radius of the calibration ring, and R_1 is the radius of each point on the object. The F-P package is described in detail in Boily (1993).

The processing of all the interferograms enabled the measurement of 12,695 velocity points covering most of the central region of Sh 170. Data points having signal-to-noise ratios smaller than 7 were rejected. The uncertainty of each velocity point varies from 0.2 km s^{-1} to 1.2 km s^{-1}.

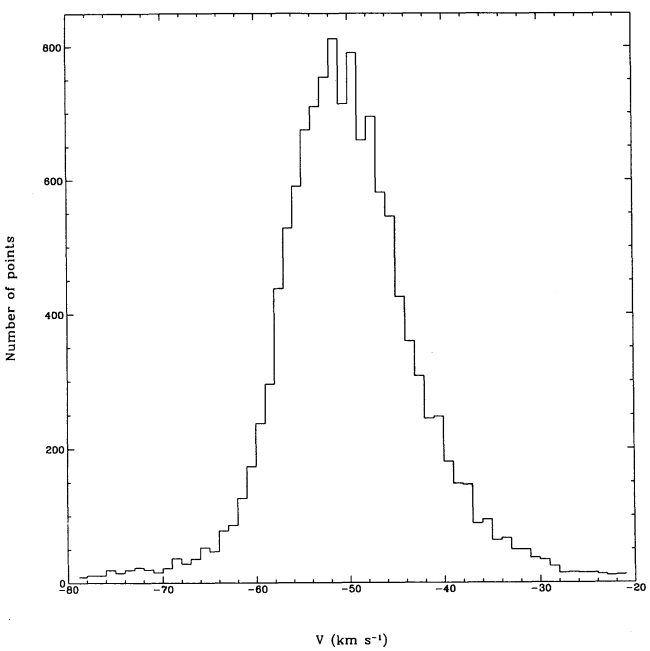

FIG. 2.—Histogram of the 12,695 Hα LSR velocities measured across Sh 170. The mean velocity is −50.10 km s^{-1} with a standard deviation of 8.70 km s^{-1}.

4. THE Hα VELOCITY FIELD

4.1. *Histogram of the LSR Velocity Points*

Figure 2 shows the distribution of the 12,695 velocity points. The mean LSR velocity is -50.10 ± 0.08 km s^{-1}. The difference with Fich et al.'s results can be explained by the area covered by their instrument; since it is smaller than Sh 170, their sampling is different than ours. The standard deviation of the distribution is 8.70 ± 0.05 km s^{-1}; this is a typical value for H II regions (Joncas & Roy 1984b, 1986). The skewness is 0.0003, indicating a symmetric distribution; it is thus clear that if Sh 170 has more than one velocity component, they are separated by less than 11 km s^{-1}. The mean LSR velocity of the H II region is blueshifted by 6.4 km s^{-1} with respect to the molecular cloud's V_{LSR}. A distribution weighted for emissivity shows exactly the same features.

4.2. *Velocity Maps*

The velocity field of Sh 170 is shown in Figure 3 in 1 km s^{-1} steps. Velocity points within 1 σ of the mean can be found all over the nebula. A north-south gradient of $\sim$1.4 km s^{-1} pc is apparent. The less negative velocities (~ -45 km s^{-1}) are in the northern part of the nebula and coincide with the molecular cloud's position and velocity (R. S. Roger 1994, private communication). The southern part of the nebula (~ -55 km s^{-1}) is the brightest region; Fich et al. (1990) may have pointed their telescope at this area.

The gradient is better illustrated in Figure 4, where "declination"-velocity and "right ascension"–velocity plots are shown. We clearly see a north-south gradient, but none east-west. Interferograms of § 2 (Table 1) have smaller signal-to-noise ratios; this explains the larger velocity dispersion found in Figure 4 around $X = 2$ pc and $Y = 2$ pc. A third velocity field representation is shown in Figure 5. A 5 × 5 grid was applied on the field, and local velocity distributions were computed. Again, the north-south gradient is apparent, as the profiles are systematically bluer in the south. We also observe red wings on almost all profiles.

Morphologically, Sh 170 has only one outstanding feature (§ 5.3): the Hα cavity. Inspection of Figures 3–5 does not reveal any special kinematical trend that could be related to this cavity. In our search for more information from our velocity field, we considered the spatial distribution of the velocity dispersion. The analysis was done by computing the standard deviation from the mean V_{LSR} in each cell of a 50 × 50 (0.65 pc × 0.65 pc) grid applied on the velocity field. Only the cells with more than 10 points were kept. This standard deviation is called "velocity dispersion" as in Joncas & Roy (1984b). Again, no systematic trends or relation with morphological features were found on the grid.

5. KINEMATICAL MODEL FOR Sh 170

5.1. *The Champagne Phase*

The Champagne model proposed by Tenorio-Tagle (1979) and detailed by Bodenheimer, Tenorio-Tagle, & Yorke (1979) successfully explains the formation and evolution of H II regions. According to this model, the ionized gas starts an explosive expansion phase when the ionization front of the H II region reaches the boundary of the parent molecular cloud. The gas is under the influence of a pressure gradient between the hot, dense, freshly ionized neutral gas and the cold, low-density intercloud medium. The gas is accelerated outward and

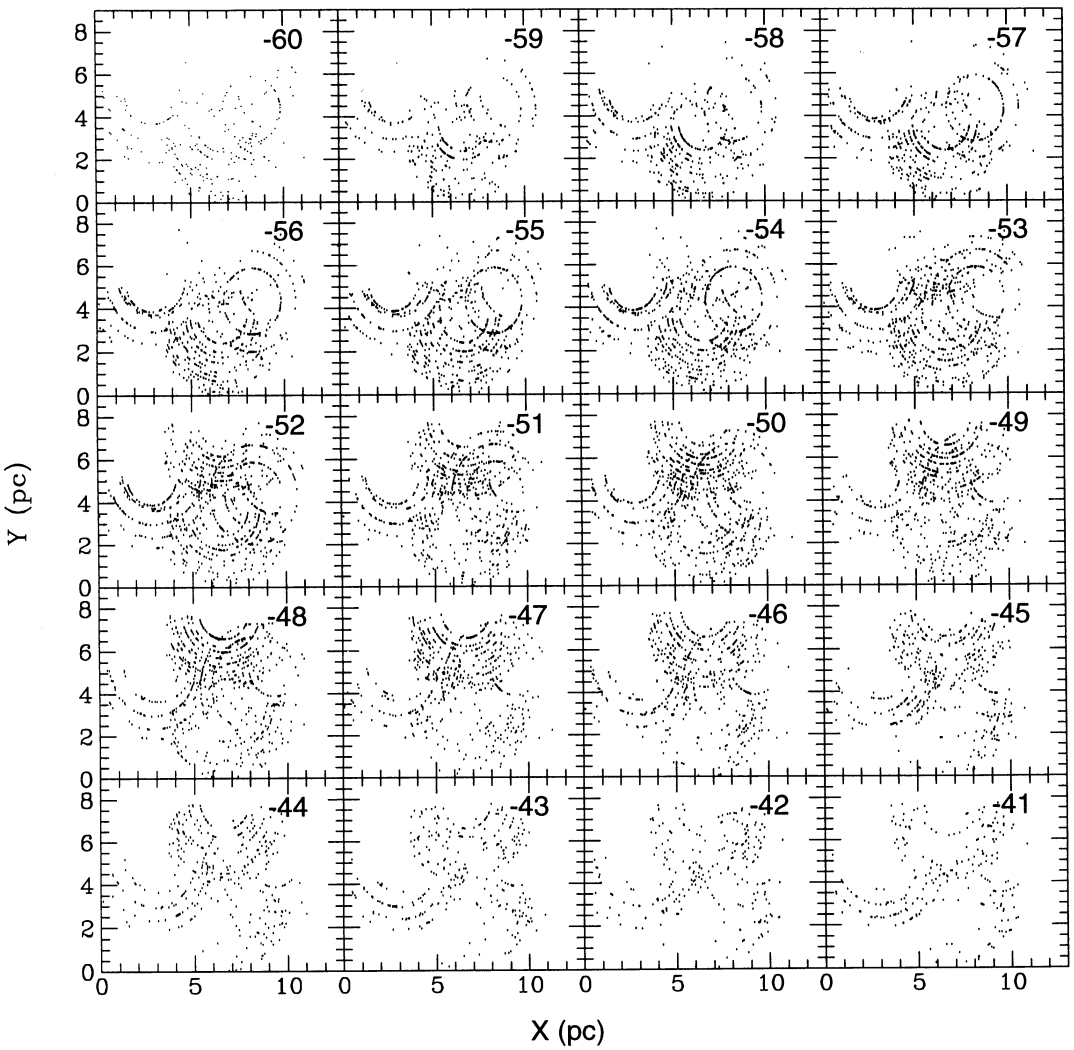

FIG. 3.—Hα LSR velocity maps of Sh 170 in steps of 1 km s^{-1}. North is up, and east is left.

a radial velocity gradient appears (Tenorio-Tagle 1979). Hence, a rarefaction wave moves into the high-density H II region. In addition, geometric dilution makes the gas density decrease from the molecular cloud to the edge of the H II region. We also expect the gas flow to be affected by a turbulent stochastic component, since the fluid is compressible, reaches supersonic speeds, and possesses a high Reynolds number. These two radial gradients make H II regions real three-dimensional gas flow problems. Therefore we must keep in mind that our observations come from a projection on the plane of the sky which implies a smearing of the information along each line of sight (Roy & Joncas 1985; Scalo 1984).

An interpretation of the velocity field characterized in figure 2 and displayed in Figures 3–5 is that the ionized gas is flowing away from its associated molecular cloud. The difference (−6.4 km s^{-1}) between the mean V_{LSR} of the ionized gas and of the molecular gas is important and could suggest a small inclination angle (Yorke et al. 1984). The circular morphology and the small radial velocity gradient could also be interpreted as a face-on geometry. A sketch of Sh 170's morphology is presented in Figure 6. It explains the north-south velocity gradient and the higher optical emission observed in the southern part of the object (Fig. 1). The red velocity wings observed in Figure 5 are probably related to ionized gas receding away from us south of the molecular cloud, since the complex is slightly tilted with respect to our line of sight.

5.2. *Modeling*

To understand the velocity field of Sh 170, a simple three-dimensional modeling of a Champagne phase H II region velocity field was done using one-dimensional density and velocity profiles as given by Tenorio-Tagle (1979, his Fig. 6*b*). The computation was done for a hemispherical H II region having a radius of 25 pc; the photoionizing star sits at $r = 0$. We use this result only as a qualitative indication of the velocity field morphology affected by the inclination angle θ of the nebula with respect to the line of sight. According to Yorke et al. (1984) and to the simple model made here, a face-on H II region with only one exciting star would have a velocity field like the one presented in Figure 7*a*. The maximum velocity is along the line of sight through the star, decreasing gradually to the edge of the nebula. This "Champagne gradient" would be coupled to an "inclination gradient" if $\theta \neq 0$ as seen in Figure 7*b*. The model also revealed that the velocity centroid dispersion is position dependent on the plane of the sky; for a face-on

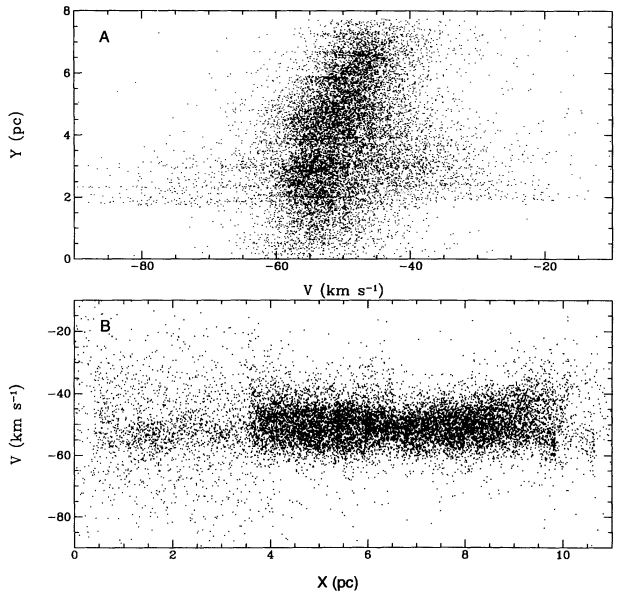

FIG. 4.—Hα LSR velocity plotted against (a) X and (b) Y. X and Y axes are oriented as in Fig. 3.

geometry, σ_c should increase from the position (x, y) of the star to the edge of the nebula.

Comparison with Sh 170's velocity field unveils a small "inclination gradient" (1.4 km s^{-1} pc) of $\theta \sim 15°$ with no "Champagne gradient." However, as for Sh 142 (Joncas & Roy 1984b), there is no spatial dependence of the velocity centroid dispersion in Sh 170. Our incomplete spatial sampling of the object may prevent us from detecting the velocity dispersion increase in the outer parts of the nebula. In addition, since the signal-to-noise ratio is systematically lower at the H II region's periphery, the observed velocity dispersion may be dominated by this effect. Therefore, the absence of the small-scale Champagne phase footprint identified here can be explained.

H II regions seem to be dynamically more complex than the Champagne phase model description. Sandford, Whitaker, & Klein (1982) showed that interaction between inhomogeneous molecular clouds and ionization shock fronts could produce jets of ionized gas at various angles in the H II region. Furthermore, stellar winds may be responsible for an important input of energy, as pointed out by Weaver, McRay, & Castor (1977). These effects may explain the absence of clear "Champagne footprints" and should be taken into account in the dynamical and kinematical description of H II regions.

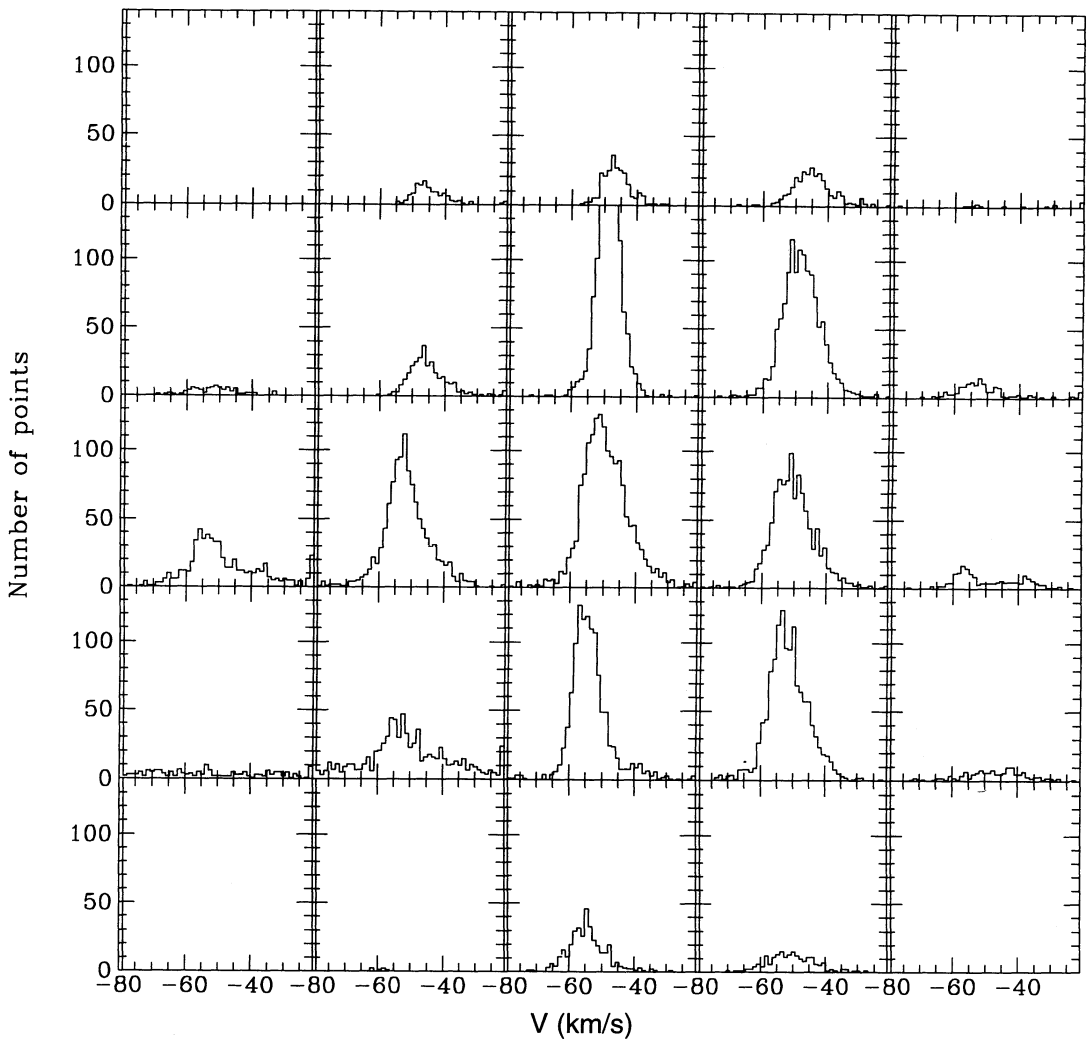

FIG. 5.—Hα LSR velocity histograms for cells on a 5 × 5 grid across Sh 170. The velocity bins are 1.2 km s^{-1}. Each cell's surface is 3.52 pc^2.

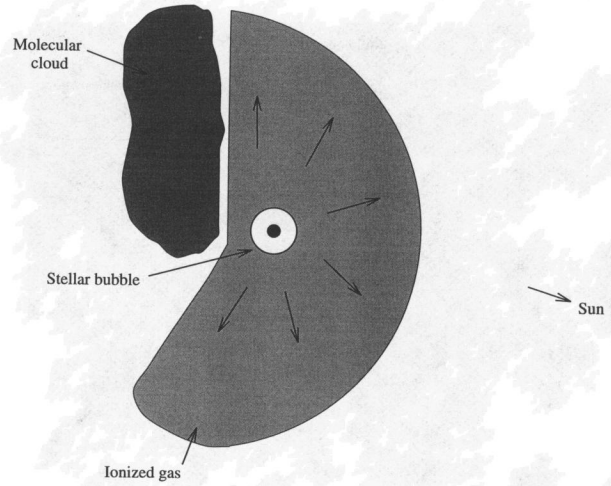

FIG. 6.—Pictorial representation of the proposed Sh 170 geometry showing the various gas components, the ionizing star DM 63°2093, and the central cavity.

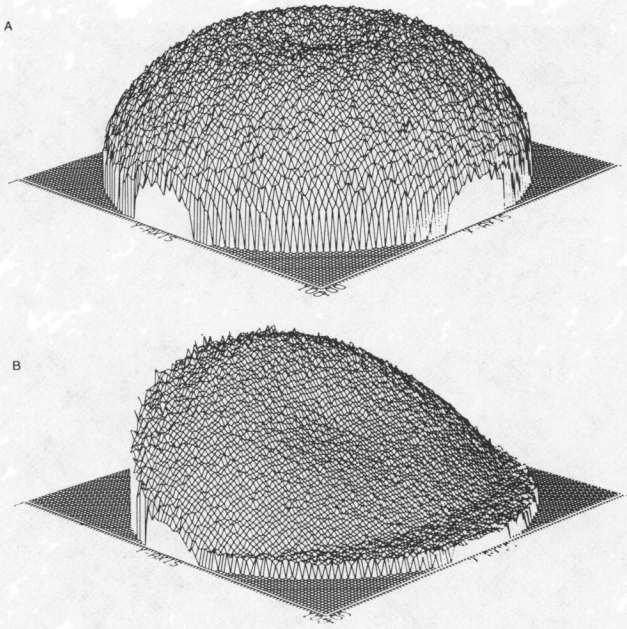

FIG. 7.—Modeling of the velocity field of an H II region as it would be seen on the plane of the sky considering the smearing of the information along each line of sight. Simple Champagne phase assumptions of three-dimensional density and velocity distribution were used (Tenorio-Tagle 1979, his Fig. 6*b*). The calculation was done for a hemispherical H II region of $r \sim 25$ pc containing one exciting star. The plane (x, y) corresponds to the plane of the sky, and the height of the surface is the velocity amplitude. The H II region's velocity field is shown (*a*) for a face-on ($\theta = 0°$) geometry and (*b*) For a $\theta = 45°$ geometry, respectively.

5.3. *Stellar Wind Cavity*

According to Figure 1 and to Roger et al. (1995), dust cannot be responsible for the emission drop in Sh 170's central region. One interpretation of this column density decrease is that a strong stellar wind creates a low-density shell around the star since molecular gas is still present to replenish the H II region. Figure 8 is an Hα monochromatic image of the central region of Sh 170, clearly showing the Hα cavity which partly surrounds DM 63°2093. The radius of this cavity is ~1 pc.

The concept of interstellar bubbles driven by a strong wind from a massive star (up to several times 10 $M_\odot$) was introduced and discussed by Castor, McRay, & Weaver (1975) and Weaver et al. (1977). They adapted the classical "à la Strömgren" expansion of H II regions (Osterbrock 1989) with the energy input of a stellar wind. The pressure exerted by the wind drives off the ionized gas, and a bubble of low-density gas surrounds the star.

Some well-known H II regions like the Rosette and Carina nebulae show a bubble morphology. They were studied by Dorland, Montmerle, & Doom (1986) in the stellar wind context using more accurate massive star evolution models than Weaver et al. (1977). The case of Sh 170 is similar and even simpler, because only one star is involved.

Dorland et al. (1986) suggested that the radius R_s of the inner shell is related to the pressure of the ionised gas P_{II} and to the wind's strength F_W by

$$F_W = 4\pi R_s^2 P_{II} , \quad (1)$$

where

$$P_{II} = 2(1 + Y) n_{II} k T_{II} . \quad (2)$$

Here n_{II} is the H II region density, T_{II} is its temperature, and Y is the ratio He/H.

Roger et al. (1995) evaluated the mass of Sh 170 at ~300 $M_\odot$. Using a diameter 13.4 pc and assuming a hemispherical geometry, we approximated the density to $n_{II} \sim 20$ cm^{-3}. Standard values were taken for the temperature and the ratio He/H, so that $Y \simeq 0.1$ and $T_{II} \simeq 8000$ K (Osterbrock 1989).

The wind's strength is evaluated using the mass-loss rate of the star. Howarth & Prinja (1989) derived an empirical relation to obtain $\dot{M}$:

$$\log \left(\frac{\dot{M}}{M_\odot \text{ yr}^{-1}} \right) = 1.69 \log (L_*/L_\odot) - 15.4 .$$

The luminosity of DM 63°2093 was derived for an O8 V star using Lang (1992) [$\log (L_*/L_\odot) = 5.23$]. Thus, we obtain a mass-loss rate of 0.27×10^{-6} $M_\odot$ yr^{-1}. The wind's strength F_W is given by

$$F_W = \dot{M} V_\infty ,$$

where V_∞ is the wind terminal velocity. Using empirical relations given by Howarth & Prinja (1989), $V_\infty \sim 2500$ km s^{-1}. Hence, we obtain $F_W \sim 4.3 \times 10^{22}$ N.

Using equations (1) and (2), the radius of the inner bubble produced by the stellar wind is evaluated at $R_s \simeq 0.83$ pc. This is in very good agreement with the cavity observed in Figure 8.

This stellar bubble description shown by Dorland et al. (1986) is valid for an H II region expanding inside a molecular cloud. As soon as the ionized gas enters the Champagne phase, its velocity is modified by the pressure gradient. Thus, the gas pressure increases and opposes the stellar wind bubble expansion. Therefore, even if the cavity observed here is well understood in terms of a standard wind bubble, the theory should be revisited considering the Champagne flow.

6. TURBULENCE

6.1. *Description*

Gas flows with high Reynolds numbers develop turbulent motions (Landau & Lifshitz 1959). Even though an analytical

FIG. 8.—Hα monochromatic photograph of the central cavity of Sh 170 obtained at the Observatoire Astronomique du Mont Mégantic. The radius of the cavity is ~1 pc (1'30").

study of turbulent fluids is impossible, Kolmogorov (1941) stated that an incompressible turbulent fluid would show a dissipationless energy cascade obeying a velocity-scale power law. Large turbulent vortices transfer their energy to smaller eddies, until viscosity or some other form of energy dissipation becomes important. At small scales, turbulent energy returns to the medium as thermal energy.

Turbulence is often represented by its energy spectrum (Fig. 9; Hinze 1975). As shown, maximum kinetic energy is obtained at k_0, which is not the size of the largest eddies, and viscous dissipation is maximum at k_d. It is in the wavenumber range $k_0 \ll k \ll k_d$, named the "inertial subrange" by Kolmogorov, that the energy transfer is dissipationless. Kolmogorov derived a relation between velocity v and scale l valid in the inertial subrange:

$$v \propto l^{1/3} . \quad (3)$$

Interstellar medium (ISM) properties suggest that it is turbulent, has an unpredictable dynamic behavior, and has multiscale coherent spatial fluctuations (Scalo 1987). In fact, the Reynolds numbers of different ISM phases (Boily 1993),

$$\mathrm{Re(H\ I)} \sim 10^5 ,$$

$$\mathrm{Re(H\ II)} \sim 10^9 ,$$

are larger than the critical value (10^2–10^4) determining the crossover to turbulence. In addition, a velocity-scale relation is observed in molecular clouds, but it is usually steeper than 1/3 (Blitz 1993).

On the other hand, several properties of the ISM might transform the energy cascade as described by Kolmogorov. The ISM is *compressible and inhomogeneous* and gas flows are often *supersonic*, implying shock wave propagation. Interaction between shock waves and turbulent fluctuations should distribute the energy dissipation over several scales. Also

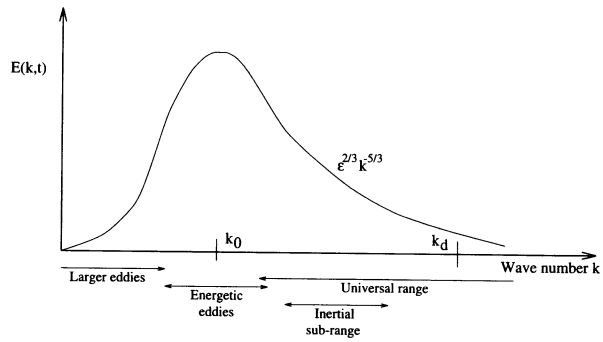

FIG. 9.—Energy spectrum $E(k, t)$ of turbulent flow adapted from Hinze (1975).

stellar winds and neutral globule effects might distribute energy injection on several scales. Furthermore, entropy fluctuations and acoustic waves, present in a turbulent compressible fluid, interact nonlinearly with turbulent fluctuations and modify the cascade (Higdon 1984). Nevertheless, it seems that compressibility does not considerably affect the energy cascade. It has been established experimentally that the energy spectrum of supersonic flows is approximately the same as for low-speed incompressible flows (Demetriades & Martindale 1983). The results suggest that modeling supersonic, turbulent compressible flows in terms of the Kolmogorov theory may be still relevant.

6.2. *Statistical Analysis*

As mentioned above, motion in a turbulent fluid is not completely random; there is some degree of correlation between neighboring points. Hence, we use statistical functions known as the autocorrelation and structure functions to measure the coherence in a turbulent fluid.

6.2.1. *Autocorrelation Function*

If some statistical properties (mean and variance) of the gas motion are not a function of position, the velocity field is considered homogeneous and stationary. In this case, it is relevant to compute the autocorrelation function (ACR). The ACR describes the coherence between points separated by a distance τ. It is defined as (Scalo 1984)

$$C(\tau) \equiv \frac{\sum [v(r) - \mu][v(r + \tau) - \mu]}{\sigma^2 N(\tau)}, \quad (4)$$

where μ is the mean velocity centroid:

$$\mu \equiv \frac{\sum v(r)}{N}, \quad (5)$$

and σ^2 is the variance:

$$\sigma^2 \equiv \frac{\sum [v(r) - \mu]^2}{N - 1}. \quad (6)$$

Here r and τ are two-dimensional vectors on the plane of the sky. The summation in equation (3) is done on all the pairs separated by τ. The μ and σ^2 are computed with the N points of the sample.

The autocorrelation function gives us information on the characteristic scales of the fluid's turbulent energy spectrum. The correlation length λ_c is the scale where:

$$C(\lambda_c) = e^{-1}.$$

Carefully, λ_c may be associated to the scale where energy dissipation processes begin to be important (Boily 1993; Kleiner 1985; Miville-Deschênes 1995).

Another important value obtained with the ACR is λ_0:

$$C(\lambda_0) = 0.$$

This is interpreted as the size of the largest energetic turbulence fluctuation (k_0 in Fig. 9). Therefore, it is the scale where the correlation vanishes. This is also the beginning of Kolmogorov's universal range (Hinze 1975).

6.2.2. *Structure Function*

The structure function (STR) is more robust than the ACR and can be used for a field only locally stationary. Its reliability is based on the fact that velocity differences are used instead of products:

$$S(\tau) \equiv \frac{\sum [v(r) - v(r + \tau)]^2}{N(\tau)}.$$

Kolmogorov predicted that for a turbulent incompressible fluid, the STR should depend on τ:

$$S(\tau) \propto \tau^{2/3}.$$

This is true for scales at which the turbulence is stationary. At larger scales, at which velocity correlations vanish, the STR should be horizontal. Intuitively, we understand this transition to occur at λ_0.

Since our observations come from a projection on the plane of the sky, there is a smearing of the velocity information along each line of sight which might affect the statistical functions. Von Hoerner (1951) has evaluated the impact of this information compression over the line of sight on the STR for a thin slab turbulent nebula. His main ideas are presented in English by O'Dell & Castañeda (1987). Von Hoerner's modeling is based on an optically thin nebula of thickness R sufficiently large that several turbulent cells are present in a given line of sight. He showed that the STR's behavior is modified for $\tau/R < 0.2$; it depends on τ like

$$S(\tau) \propto \tau^{5/3}.$$

6.2.3. *Systematic Trend Correction*

As mentioned above, a valid statistical analysis of velocity fluctuation has to be done on a homogeneous and stationary velocity field. This condition will be fulfilled if all systematic trends are removed, leaving a velocity field with mean and variance spatially independent. This removal is a difficult task for H II regions (§ 5.1). These caveats must be kept in mind when the results are analyzed, since the statistical functions are affected by them (especially the ACR). A simple way to proceed is to fit a two-dimensional polynomial to the data. On the other hand, spectral filtering techniques (Kleiner 1985; Miesch & Bally 1994) are better suited to extract systematic components from the velocity field. These techniques were impossible to apply to our data set; our F-P observations were obtained in a discrete mode resulting in a two-dimensional matrix with noncontinuous sampling, preventing us from using convolution techniques (i.e., a Zurflueh filter) to extract large-scale gradients or wavelet transform for the analysis of turbulence.

Therefore, a polynomial fit was applied to remove the large-scale gradient in the data set. The technique used to avoid the "noncontinuous sampling problem" was to bin the velocity field. A grid pattern was applied on the velocity field. Each cell was attributed the mean of the velocity points falling in it or, if there were none, the mean velocity of the sample. A fourth-order polynomial function was fitted on that grid and subtracted from the velocity field. The most important parameter in this operation is the mesh size of the grid pattern. The choice of the cell's dimension is crucial because it is directly related to the scale of the systematic component extracted; a small grid size fit will remove both the large-scale gradient and part of the velocity fluctuations. Velocity field inspection with plots like those presented in Figure 4 were used to determine the optimum grid size. We also used the fact that the ACR is particularly sensitive to large-scale trends. Contrary to the ACR, the STR was remarkably stable against the successive

filterings that were done for different mesh sizes. Intuitively, one would believe that the turnoff of the STR should correspond to λ_0 (confirmed by Boily 1993). In fact, these two values indicate the scale where correlations vanish. Therefore, we used this characteristic of the statistical functions to determine the optimum grid size. It was thus found that a 20×20 grid removes adequately the north-south gradient and leaves an ACR with a λ_0 value at approximately the same scale than the STR's turnoff.

6.2.4. *Sh 170*

After the removal of the large-scale gradient, the ACR and STR were computed with the remaining velocity fluctuations of Sh 170. The functions are shown in Figures 10*a* and 10*b*, respectively. From Figure 10*a*, we obtain $\lambda_c = 0.03 \pm 0.02$ pc and $\lambda_0 = 0.08 \pm 0.01$. The spatial resolution is 0.011 pc (1″ at 2.3 kpc).

The Kolmogorov exponent obtained from the structure function is 0.8 ± 0.1. The uncertainty for the STR was computed using the bootstrap technique (Efron & Tibshirani 1986). As seen in Figure 10*b*, the turnoff of the STR appears at 0.07 pc which approximately corresponds to λ_0. All these values are in agreement with the results of Joncas & Boily (1995) obtained from four H II regions. On the other hand, the STR results of O'Dell (1986) and O'Dell, Townsley, & Castañeda (1987) are noticeably different from ours. This discrepancy comes from the fact that they did not remove the large-scale gradients from their velocity fields. In our case, although the filtering technique used has disadvantages, the large-scale gradient seems to have been successfully removed. In this context, our computation of the autocorrelation and structure functions are reliable.

Measuring λ_c in a homogeneous velocity field can be interpreted as confirming the presence of turbulence. Our results join the assumption of Louise & Monnet (1970), Roy & Joncas (1985), O'Dell (1986), and O'Dell & Castañeda (1987) that H II regions have a turbulent velocity field. On the other hand, one could doubt the validity of the correlation length λ_c computed here. Its value is only twice our spatial resolution. Nevertheless, as pointed out by Joncas & Boily (1995), every result converges to a unique value ($\lambda_c \approx 0.02$) for H II regions with different resolution, distance, and geometry. However, this value must still be used with caution.

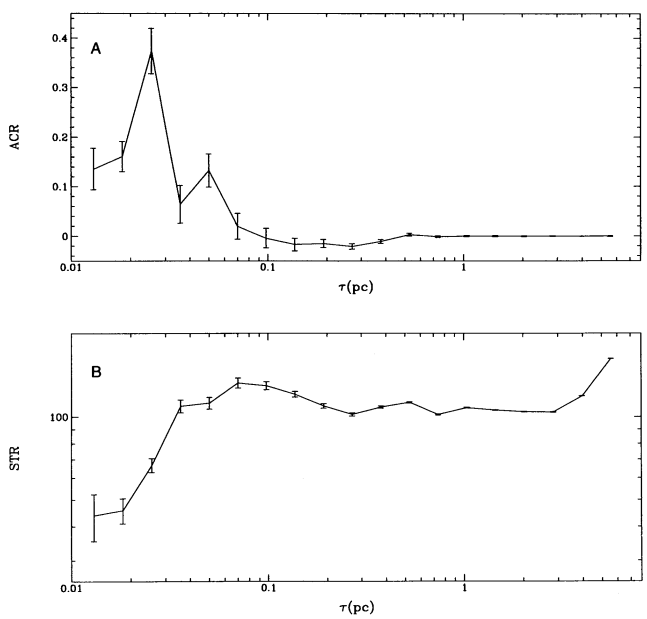

FIG. 10.—The two-point autocorrelation (*a*) and structure (*b*) functions, where τ is the separation between velocity pairs. Vertical bars correspond to the statistical uncertainty (confidence level of 99%).

The structure function obtained here is coherent with the ACR results. The slope of the STR is indeed positive at small velocity separations and becomes ~ 0 at larger values. The transition is at 0.07 pc and indicates that the size of the largest energetic eddies is ~ 0.07 pc. It is worth noting that turbulence is present at larger scales; energetic eddies are not the biggest fluctuations in a turbulent flow (Fig. 9). Considering a face-on hemispherical geometry and a diameter of 13.4 pc, Sh 170's depth is $R \sim 6.5$ pc. Since the slope of the STR is positive for $\tau < 0.07$ pc, the turbulent scales characterized here are in the $\tau/R < 0.2$ range. At these scales, von Hoerner's model predicts a 5/3 slope. To bring the STR closer to a 2/3 slope ($\tau/R > 0.2$), we should consider $R \sim 0.1$ pc which is hard to reconcile with a Champagne phase H II region with Sh 170's diameter. Although the presence of turbulence in Sh 170 is again confirmed, we believe that the energy cascade is not "à la Kolmogorov." H II regions are not made of an incompressible fluid, and energy input may be occurring at different scales (e.g., a stellar wind doubling with a Champagne shear flow), explaining the difference between our results and von Hoerner's modeling.

We also pointed out that statistical functions results obtained with centroid velocities may not give an exact representation of the turbulent medium in the H II region context. Evaluating line-of-sight information compression effects is a major task, since the reliability of ACR and STR analysis can only be checked if we have an H II region three-dimensional model including a partly supersonic expansion phase, shock waves, stellar winds, and density and velocity fluctuations at our disposal.

6.3. *Dispersion of LSR Velocities*

A study of velocity dispersions obtained after the removal of the large-scale gradient is relevant in the Champagne phase (§ 5.2) and turbulence analysis. But we first have to make an important distinction between the global velocity dispersion of an object and the dispersion obtained with velocity centroids.

The velocity point observed at position (x, y) on the plane of the sky with F-P interferograms is the velocity centroid $v_c(x, y)$ of the emitted line profile. For optically thin emission lines (like Hα), $v_c(x, y)$ is the most probable velocity of the gas along the line of sight at (x, y)

$$v_c(x, y) = \frac{\int_{-\infty}^{\infty} I(u; x, y) u \, du}{\int_{-\infty}^{\infty} I(u; x, y) du},$$

where $I(u; x, y)$ is the emergent emission at velocity u from position (x, y), integrated along the line of sight; $v_c(x, y)$ is not equal to the mean velocity along the line of sight (x, y), since H II regions are affected by three-dimensional density, velocity, and possibly temperature gradients. The velocity centroid is representative of the gas behavior along the line of sight. Considering that gasdynamical conditions vary in H II regions, velocity centroids are dependent on position.

Figure 2 shows the distribution of the N_c measured velocity centroids; the dispersion σ_c extracted from this histogram is

the fluctuation of the velocity centroid $v_c(x, y)$ about the mean $\langle v_c \rangle$.

The true mean velocity of an object is given by

$$\langle v_t \rangle \equiv \sum \frac{v(x, y, z)}{N_t},$$

where x and y define the plane of the sky, z is its depth, and N_t is the total number of velocity points in the volume. The mean velocity centroid $\langle v_c \rangle$ is equal to the true mean velocity of the object $\langle v_t \rangle$ if the distribution of velocity centroid is symmetric. In our case, $\langle v_t \rangle \simeq \langle v_c \rangle$ because the skewness of Figure 2 is ~ 0. On the other hand, the true velocity dispersion σ_t of the gas is not equal to σ_c. In fact, the true velocity dispersion of the gas, given by

$$\sigma_t \equiv \sqrt{\sum \frac{[v(x, y, z) - \langle v_t \rangle]^2}{N_t - 1}},$$

is related to the velocity centroid dispersion if one knows the internal velocity dispersion (Kleiner 1985):

$$\sigma_t^2 = \sigma_i^2 + \sigma_c^2,$$

where σ_i^2 is the mean variance of the velocities along each line of sight:

$$\sigma_i^2 \equiv \left\langle \sqrt{\sum \frac{[v(x, y, z) - \langle v(x, y, z) \rangle_z]^2}{N_i - 1}} \right\rangle_{x, y}.$$

Thus, the use of velocity centroids underestimates the velocity dispersion of the nebula. Since our data preclude the measurement of an effective line width, it is impossible to determine here the amplitude of σ_i and thus evaluate σ_t. In § 5.2 we discussed the relevance of analyzing the spatial behavior in the context of the velocity dispersion in H II region Champagne phase analysis. This is demonstrated by the Fountain, Gary, & O'Dell (1979) Hα line width measurements of 700 points on the Rosette nebula which is morphologically similar to Sh 170. Their data show a radial increase of the line width from the center to the boundary of the object. This increase can be interpreted as the radial dependence of σ_i resulting from the expansion of the nebula. We are now convinced that the measurement of σ_i is imperative for the kinematical analysis of an H II region.

6.4. *Scaling Law*

Many authors (i.e., Larson 1981) have associated a relation like

$$\Delta V \propto l^{\gamma}$$

to the presence of turbulence in the observed fluid. In his 1981 paper, Larson treats numerous molecular clouds obtaining $\gamma = 0.38$. He associated this result to the "one-third" law of Kolmogorov for incompressible turbulence (eq. [3]). The scales used in his analysis cover 0.5 pc to 60 pc. Note that ΔV (the total line width of the region observed) is equivalent to σ_t. In this context, the σ_c-σ_t distinction made above is very important.

Even though σ_t is unavailable to us, a relation between σ_c and scale l may give some information on the velocity fluctuations in the ionized gas flow. Hence, several grids of different mesh size were applied on our velocity field. The mean velocity and the velocity dispersion were computed for cells with more than 10 points. We related each mesh size with its most probable velocity dispersion and obtained the relationship shown in Figure 11. A linear regression (Isobe et al. 1990) using the bootstrap (Efron & Tibshirabi 1986) technique to derive the uncertainties gave

$$\sigma(V) \propto l^{0.30 \pm 0.03}.$$

This result was the same before and after the removal of the large-scale gradient (§ 6.2.3). Such a relation has been observed for Sh 142 ($\gamma = 0.30 \pm 0.02$; Roy & Joncas 1985) and M17 ($\gamma = 0.25 \pm 0.04$; Joncas & Roy 1986). These results are in good agreement with those presented here. On the other hand, we note that the use of σ_t may change the slope of the relation. The similarity between the H II region and molecular cloud exponents may be fortuitous.

As shown by Kleiner & Dickman (1985), a power-law relationship between internal velocity dispersion σ_i and scale should be observed in the inertial subrange of turbulence as defined by Kolmogorov:

$$\sigma_i \propto l^{\gamma}.$$

On the other hand, the statistical analysis made here suggests a narrow inertial range for Sh 170 (from 0.02 pc to 0.07 pc), while the σ_c versus l relation presented here expands far beyond this range. Molecular clouds exhibit the same behavior; Larson's work indicates that this relation is valid as far as 60 pc, while estimations of the largest turbulent eddies in molecular clouds is under 1 pc (Kleiner 1985). This indicates clearly why the scientific community hesitates in interpreting Larson's relation in terms of turbulence. The technique used here is also known as "quadrat counts," but its statistical interpretation is difficult (Ripley 1981). So this result is only given for comparison purposes, and no physical quantitative information will be deduced. As pointed out by Scalo (1984), autocorrelation and

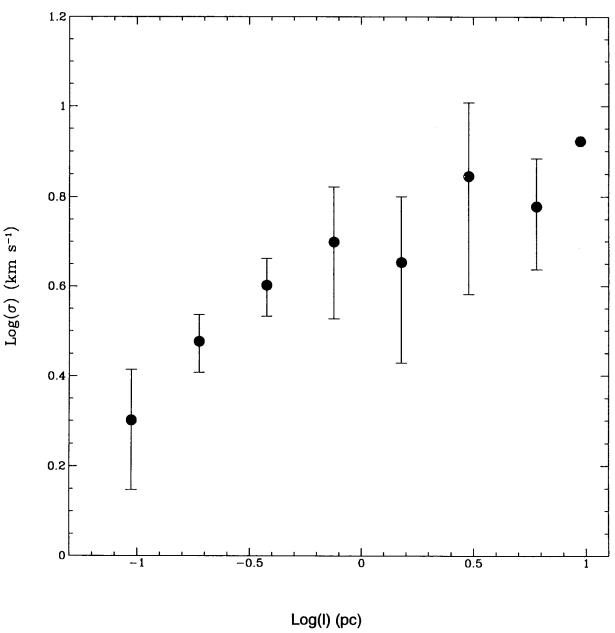

FIG. 11.—Logarithmic plot of the velocity dispersion as a function of mesh size on the nebula. The width of each cell has been converted into parsecs, assuming a distance of 2.3 kpc for Sh 170. Vertical bars correspond to the statistical uncertainty (confidence level of 80%).

structure functions are more reliable tools for the analysis of velocity fluctuations.

7. CONCLUSION

A total of 12,695 Hα radial velocity points have been measured across the H II region Sh 170 using an F-P camera. The large-scale velocity field analysis is in agreement with an H II region experiencing a Champagne phase which we see with a small inclination angle with respect to the line of sight. On the other hand, small-scale analysis revealed that kinematical models should be polished to take into account other sources of mechanical energy. A central cavity was observed and successfully interpreted as a stellar wind bubble. A power-law relation between velocity dispersion and scale that may be interpreted as indicating the presence of turbulence motions was obtained. Furthermore, studies with two-point correlation functions clearly confirm the presence of turbulence extending over a small range of scales. The size of the largest energetic turbulent fluctuation for this object is ~ 0.07 pc, and energy dissipation becomes important at scales ~ 0.03 pc. These results are in good agreement with previous studies.

We thank Steve Godbout for staying up late to provide us with an appreciated picture of Sh 170's cavity, and R. S. Roger and P. E. Dewdney, who kindly made their data available to us. Discussions with Jean-René Roy, Edouard Boily, Richard N. Henriksen, Anthony J. Moffat, and Sébastien Lépine were very helpful. Guy Plante, Rosanne Chabot, and Charlie Haden helped in preparing this manuscript. The Fond FCAR du Québec and the National Science and Engineering Research Council of Canada provided funds to support this research project.

REFERENCES

Blitz, L. 1993, in Protostars and Planets III, ed. E. H. Levy & J. I. Lumine (Tucson: Univ. Arizona Press), 125
Bodenheimer, P., Tenorio-Tagle, G., & Yorke, H. W. 1979, ApJ, 233, 85
Boily, E. 1993, Ph.D. thesis, Université Laval
Castor, J., McRay, R., & Weaver, R. 1975, ApJ, 200, L107
Demetriades, A. P., & Martindale, W. R. 1983, Phys. Fluids, 26, 397
Dorland, H., Montmerle, T., & Doom, C. 1986, A&A, 160, 1
Efron, B., & Tibishirani, R. 1986, Stat. Sci., 1, 54
Fich, M., & Blitz, L. 1984, ApJ, 279, 125
Fich, M., Treffers, R. R., & Dahl, G. P. 1990, AJ, 99, 622
Fishel, D., & Feibelman, W. A. 1973, ApJ, 180, 801
Fountain, W. F., Gary, G. A., & O'Dell, C. R. 1979, ApJ, 229, 971
———. 1983a, ApJ, 269, 164
———. 1983b, ApJ, 273, 639
Higdon, J. C. 1984, ApJ, 285, 109
Hinze, J. O. 1975, Turbulence (New York: McGraw-Hill)
Howarth, I. D., & Prinja, R. K. 1989, ApJS, 69, 527
Hunter, D. A., & Massey, P. 1990, AJ, 99, 846
Isobe, T., Feigelson, E. D., Akritas, M. G., & Babu, G. J. 1990, ApJ, 364, 104
Israel, F. P. 1978, A&A, 70, 769
Joncas, G., & Boily, E. 1995, in preparation
Joncas, G., Durand, D., & Roger, R. S. 1992, ApJ, 387, 591
Joncas, G., & Roy, J. R. 1984a, PASP, 96, 263
———. 1984b, ApJ, 283, 640
———. 1986, ApJ, 307, 649
Kaplan, S. A., & Pikelner, S. B. 1970, The Interstellar Medium (Cambridge: Harvard Univ. Press)
Kleiner, S. C. 1985, Ph.D. thesis, Univ. Massachusetts
Kleiner, S. C., & Dickman, R. L. 1985, ApJ, 295, 466
Kolmogorov, A. N. 1941, Dokl. Akad. Nauk SSSR, 30, 301
Lahulla, J. F. 1985, A&AS, 61, 537
Landau, L. D., & Lifshitz, E. M. 1959, Fluid Mechanics (Oxford: Pergamon)
Lang, K. R. 1992, Astrophysical Data: Planets and Stars (New York: Springer)
Larson, R. 1981, MNRAS, 186, 479
Louise, R., & Monnet, G. 1970, A&A, 8, 468
Miesch, M. S., & Bally, J. 1994, ApJ, 429, 645
Miville-Deschênes, M. A. 1995, M.Sc. Thesis, Université Laval
Mufson, S. I., Fountain, W. F., Gary, G. A., Howard, W. E., III, O'Dell, C. R., & Wolff, T. M. 1981, ApJ, 248, 992
Myers, P. C. 1987, in Interstellar Processes, ed. D. J. Hollenbach & H. A. Thronson (Dordrecht: Reidel), 71
O'Dell, C. R. 1986, ApJ, 304, 767
O'Dell, C. R., & Castañeda, H. O. 1987, ApJ, 317, 686
O'Dell, C. R., Townsley, L. K., & Castañeda, H. O. 1987, ApJ, 317, 676
Osterbrock, D. E. 1989, Astrophysics of Gaseous Nebula and Active Galactic Nuclei (Mill Valley: University Science Books)
Ripley, B. D. 1981, Spatial Statistics (New York: Wiley)
Roger, R. S., Dewdney, P. E., & McCutcheon, W. B. 1995, in preparation
Roy, J. R., & Joncas, G. 1985, ApJ, 288, 142
Sandford, M. J., Whitaker, R. W., & Klein, R. I. 1982, ApJ, 260, 183
Scalo, J. M. 1984, ApJ, 277, 556
———. 1987, in Interstellar Processes, ed. D. J. Hollenbach & H. A. Thronson (Dordrecht: Reidel), 349
Sharpless, S. 1959, ApJS, 4, 257
Tenorio-Tagle, G. 1979, A&A, 71, 59
von Hoerner, S. 1951, Z. Astrophys., 30, 17
Weaver, R., McRay, R., & Castor, J. 1977, ApJ, 218, 377
Wilson, T. L., Fazio, G. G., Jaffe, D., Kleinmann, D., Wright, E. L., & Low, F. J. 1959, A&A, 76, 86
Wouterloot, J. G. A., & Brand, J. 1989, A&AS, 80, 149
Yorke, H. W., Tenorio-Tagle, G., & Bodenheimer, P. 1984, A&A, 138, 325